Indonesian Physical Review
Volume 08 Issue 02, May 2025
P-ISSN: 2615-1278, E-ISSN: 2614-7904

Analysis of Lines Formation Produced by Electrohydrodynamic Jet Printing for Terahertz (THz) Metamaterials Fabrication

Ayodya Pradhipta Tenggara[1*], Hadi Teguh Yudistira[2], Brian Godwin Mtei[3], Doyoung Byun[3]
[1]*Faculty of Engineering, Universitas Gadjah Mada, Yogyakarta, Indonesia*
[2]*Faculty of Industrial Technology, Institut Teknologi Sumatera (ITERA), Lampung, Indonesia*
[3]*Department of Mechanical Engineering, Faculty of Engineering, Sungkyunkwan University, Suwon, South Korea*

Corresponding Author's E-mail: ayodya.p.t@ugm.ac.id

Article Info

Article info:
Received: 15-11-2024
Revised: 15-04-2025
Accepted: 18-04-2025

Keywords:
Electrohydrodynamic Jet Printing; Microfabrication; Line Formation; Split Ring Resonator; Metamaterials

How To Cite:
A. P. Tenggara, H. T. Yudistira, B. G. Mtei, and D. Byun, "Analysis of Lines Formation Produced by Electrohydrodynamic Jet Printing for Terahertz (THz) Metamaterials Fabrication", Indonesian Physical Review, vol. 8, no. 2, p 448-462, 2025.

DOI:
https://doi.org/10.29303/ipr.v8i2.433.

Abstract

Electrohydrodynamic (EHD) jet printing has revolutionized semiconductor manufacturing technologies to fabricate high resolution materials pattens (metal, dielectric, or semiconductors) in small size. This technology can reduce excessive materials usage in conventional semiconductor lithographic technologies, such as photolithography or electron beam lithography, so that it can be categorized as a green manufacturing technology. EHD jet printing has a capability to fabricate resonant terahertz metamaterial. Resonant terahertz metamaterial contains metal structures in micrometer sizes patterned on dielectric substrate. The metal structures are arranged periodically to generate resonances in specific frequencies, which are beneficial for several applications, such as biosensing, chemical sensing, and terahertz optical modulators for future communication devices. To make a high resolution and repeatable structures, EHD jet printing faces two main problems, i.e. the drop coalescence problem and the charge problem. The charging problem can be solved by removal of substrate charges using ionizer. However, the drop coalescence problem is a type of complex problem that needs to be studied and optimized systematically to produce repeatable and reliable terahertz resonant metamaterial structures, which is electric split ring resonator (ESRR). The objective of this research is to investigate to the formation stability of dots and lines produced by the EHD jet printing. We used EHD jet printing through the Drop on Demand (DoD) method to deposit droplets from metal nanoparticle ink with various volumes on dielectric substrates with different thickness. Several parameters were investigated, i.e. the droplet volume, the droplet spacing, and the substrate thickness. The results showed that by increasing the deposited droplet volumes and decreasing the substrate thickness, the stability of line formation was improved. Moreover, the stability analysis of line formation revealed that by using the bigger volume, the minimum printing speed to make uniform line was decreased, because the bigger droplet volume gave smaller contact angle. The results also showed that the uniformity of metamaterials patterns could be improved by using the smaller width.

Copyright (c) 2025 by Author(s), This work is licensed under a Creative Commons Attribution-ShareAlike 4.0 International License.

Introduction

Electrohydrodynamic (EHD) jet printing has emerged as a transformative technique for fabricating microscale and nanoscale structures, including electronic circuits, sensors, or dielectric patterns for various types of solar cells [1], terahertz metamaterials [2, 3] or living cells [4]. Unlike conventional inkjet methods constrained by nozzle size, EHD jet printing leverages electric fields to generate droplets as small as 10 μm^3—over two orders of magnitude finer than thermal/piezoelectric alternatives [5]. This capability stems from the formation of a Taylor cone under high electric potentials which creates a thin-extruded jet from the nozzle giving it the ability to go much lower than the limits of the nozzle diameter, which in-turn enables precise deposition of functional materials [6, 7]. Among EHD techniques, droplet-on-demand (DoD) printing excels at patterning intricate 2D/3D geometries [8-10], yet its practical adoption is hindered by unresolved challenges tied to charge dynamics and fluid stability.

Despite its advantage in making tiny and delicate micro/nanostructures, DoD deposition technique of EHD jet printing has two main drawbacks. The first drawback is related to the influence of the charge on the substrate, which may affect the electric field distribution and may interrupt the subsequent printing behavior [8-10]. When charges exist on the substrate, the route of the flying liquid drops was not straight because the electric field distribution between the nozzle and the substrate was not uniform. Consequently, the deposited drops deviated from their target spots. Depending on the charge and applied voltage, flying liquid drops may deflect, reflect, or retreat to the liquid meniscus on the nozzle. The flying drops around the conductive substrate was more stable than the flying drops around the dielectric substrate, because on the conductive substrate the remaining charges could be easily removed [8, 9]. Another option to solve this charge problem is by applying AC voltage only on the substrate [10].

While prior studies have explored general EHD printing mechanics [11], knowledge gaps persist in understanding how substrate-dependent charge interactions influence droplet behavior. For instance, residual charges on dielectric substrates disrupt electric field uniformity and homogeneity, causing droplet deflection or retreat [12, 13]. Although conductive substrates mitigate this via charge dissipation [14], most functional applications (e.g., THz metamaterials) require dielectric surfaces like SiO_2 or glass [15, 16]. Compounding this issue, existing stability models for line formation [15, 17] neglect charge effects, as they derive from non-EHD systems using neutral droplets. This oversight is critical: EHD-generated droplets retain inherent charges, altering coalescence dynamics and line morphology [14]. Furthermore, the role of substrate thickness in modulating charge accumulation and printing stability remains unexplored, despite its impact on electric field distribution [18, 19].

This study systematically investigates charged droplet behavior on thin (SiO_2) and thick (glass) dielectric substrates, addressing two core problems: (i) the mechanism of residual charges and substrate thickness that affect dot placement accuracy; and (ii) Identification of parameters that govern line stability when printing charged droplets across dielectric surfaces. By analyzing droplet volumes (18–4900 μm^3), spacing, and substrate motion, we identify optimal conditions for stable patterning. Our findings reveal that thicker substrates exacerbate charge retention, destabilizing dot formation—a phenomenon mitigated by larger droplet volumes. Conversely, line uniformity depends primarily on printing velocity, with minimal substrate

thickness effects. These insights advance EHD printing for THz metamaterials and flexible electronics, where precision on dielectric surfaces is paramount.

Experimental Method

The schematic of the EHD jet printing system is shown in Figure 1. Several components were included in the system, such as a micro syringe pump, a glass capillary nozzle, a function generator, and an axis motor. The micro syringe pump was used to supply liquid ink from a syringe into the glass capillary nozzle. The glass capillary nozzle was used to supply the ink to produce flying drops. In this experiment, glass capillary nozzles with different inner diameters were used: 6 µm, 15 µm, and 50 µm. Harima NPS-J silver nanoparticles liquid solution was used as the ink. The metal content, viscosity, and surface tension of the ink were 63.1 wt%, 8.2 x 10^{-3} Pa·s, and 27 x 10^{-3} N/m, respectively.

A droplet was formed by the accumulation of flying drops on a spot area on the substrate [20, 21]. Larger droplet volumes on a targeted spot area could be achieved when more flying drops were produced, which could be controlled by adjusting the pulse width of the pulsed DC signal [22]. Pulsed DC signals were generated by the function generator and were used to control the DoD jetting process. The parameters of these signals included the pulse peak voltage, the bias voltage, the pulse width, and the period. The bias voltage was used to maintain the charge in the meniscus, while the pulse peak voltage determined the jetting performance at the nozzle tip. The pulse width affected the number of flying drops generated from the meniscus. The spot area was determined by the electric field distribution; if the spot area was too large, the droplet formation would be less uniform.

In the experiment, the nozzle-substrate distance was maintained at 30 µm, 30 µm, and 75 µm for nozzles with diameters of 6 µm, 15 µm, and 50 µm, respectively. Under these working distances, the printing processes were stable, producing relatively uniform droplets on the substrates. For a nozzle-substrate distance of 30 µm, the pulse peak voltage, bias voltage, and pulse width were set at 0.5 kV, 0.1 kV, and 1 ms, respectively. For a distance of 75 µm, these parameters were set at 0.75 kV, 0.1 kV, and 1 ms, respectively. The volume of each droplet produced by nozzles with inner diameters of 6 µm, 15 µm, and 50 µm was 18 μm^3, 260 μm^3, and 4900 μm^3, respectively. The volume measurements were conducted using a NanoSystem Three-Dimensional Profiler. Two dielectric substrates with different thicknesses were used: SiO_2 and glass, with thicknesses of 200 µm and 400 µm, respectively. The substrates were initially cleaned with ethanol to effectively remove surface charges.

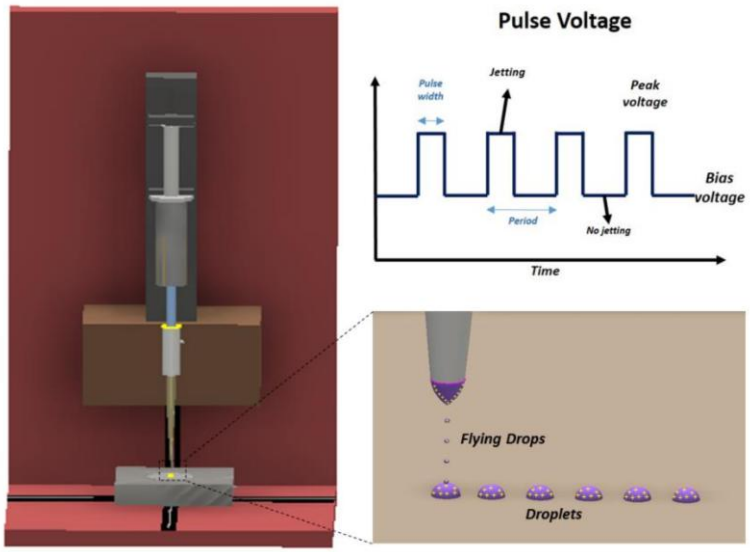

Figure 1. The schematic of the DoD EHD jet printing system

Figure 2 shows the illustration of DoD EHD jet printed dots and lines by varying the droplet spacing. Increasing the droplet spacing could create separation of droplets, while decreasing the droplet spacing could connect them. Four types of patterns could be obtained: isolated dots, pair dots, a uniform line, and a bulged line. Isolated dots were formed when the droplet spacing was much larger than the droplet diameter. Pair dots were formed when two or three droplets emerged together due to a weak fluid force on their boundary, creating a flow toward the neighboring droplet and resulting in short, discontinuous lines. A uniform line or a bulged line was formed when the droplet spacing was much smaller than the droplet diameter.

In this research, a droplet deposited on a substrate was modeled as a spherical cap because the gravitational force was not significant, as indicated by the low value of its Bond number, which was significantly less than 1. The Bond number is a dimensionless number that compares the gravitational force with the surface tension force, as expressed in equation (1), where ρ, g, d_{eqm}, and σ represent the liquid density, the gravitational acceleration, the droplet diameter, and the surface tension of the liquid ink, respectively.

$$Bo = \frac{\rho g d_{eqm}}{\sigma} \tag{1}$$

Figure 2(b) shows the illustration of the basic parameters, i.e., d_{eqm}, w, θ_a, θ, and p. d_{eqm} is the equilibrium diameter of the droplet on the substrate. w is the width of the line generated after the droplet coalescence; θ_a is the advancing contact angle, which is the contact angle between the droplet and the substrate; θ is the contact angle between the printed line and the substrate.

To represent the droplet spacing, two parameters were used: the pitch (p) and the normalized pitch ($p*$), as expressed in equation (2). The droplet spacing could be controlled by adjusting the printing velocity or the period of the pulse signal.

$$p^* = \frac{p}{d_{eqm}} \tag{2}$$

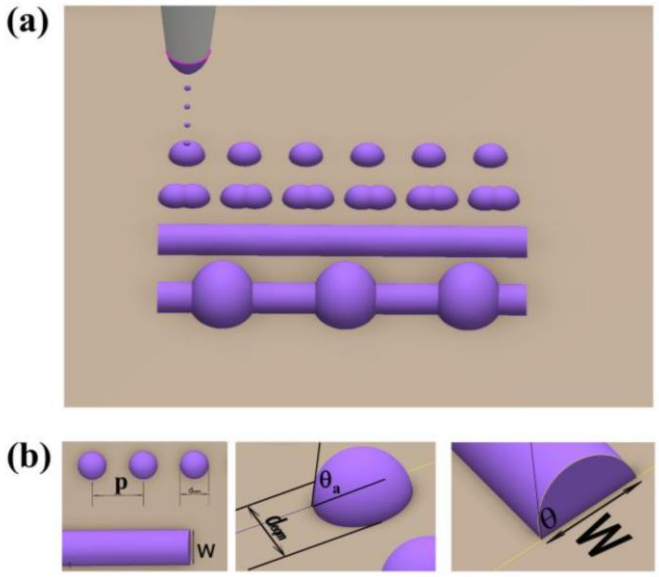

Figure 2. (a) The illustration of dots and lines formations. (b) The description of the formation parameters

Result and Discussion

Figure 3 shows the optical microscopic images of the printed samples on the SiO_2 substrate using droplets with a volume of 18 µm³ for each droplet were used. The droplet spacing was varied between 1 µm and 10 µm. Uniform lines were obtained for droplet spacings between 4 µm and 6 µm. When the droplet spacing was more than 6 µm, pair dots or separated dots were formed. Conversely, when the droplet spacing was less than 4 µm, bulged lines were formed. Figures 2-3(b) shows the three-dimensional profiles of lines and separated dots of the printed samples.

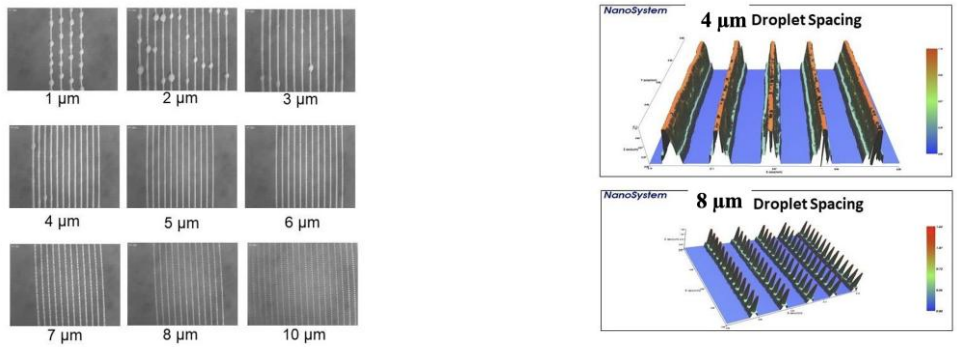

(a) (b)

Figure 3. (a) The optical microscopic images of the printed samples using droplets with 18 µm³ volume for each droplet on SiO_2 substrate by varying the droplet spacing, (b) 3D profiles of lines and separated dots of the printed samples using dots with 18 µm³ volume for each droplet on SiO_2 substrate by varying the droplet spacing.

Figures 4(a) and (b) show the printed results on the SiO_2 substrate and the glass substrate, respectively, by varying the droplet spacing and the droplet volume. The results indicate that the printing on the SiO_2 substrate was more uniform than on the glass substrate. The SiO_2 substrate was thinner than the glass substrate, allowing the remaining charges on the SiO_2 substrate to be more easily removed. Consequently, the electric field distribution around the SiO_2 substrate was more uniform than that around the glass substrate.

The non-uniformity of the electric field distribution around the glass substrate affected the route of the flying drops [8, 9]. When the routes of the flying drops were less straight, the area of the deposition target became larger, and deviations in the deposited droplets occurred more frequently. These phenomena can be observed clearly in the pair dots and isolated dots printed on the glass substrate with a droplet volume of 18 μm^3, as shown in the Figure 4(b). Increasing the droplet volume could reduce the deviation of the droplets. These phenomena can be observed clearly in the pair dots and isolated dots printed on the glass substrate with a droplet volume of 18 μm^3, as shown in the Figure 4(b). Increasing the droplet volume could reduce the deviation of the droplets. This phenomenon shows clearly that thinner dielectric substrate (SiO_2) dissipates charges faster than thicker dielectric substrate (glass), as shown clearly by the printing results.

The Rayleigh-Plateau instability occurs for all droplet volumes, not only in small droplet volumes but also in large droplet volumes, when the charges contained inside the droplets exceed the charge amount defined by the Rayleigh limit [8, 9]. However, in the case of larger droplet volumes, most of the *satellite droplets* produced by the Rayleigh-Plateau instability that were deposited on the substrate could merge with the main dots, resulting in larger dots with fewer satellite depositions on the substrate.

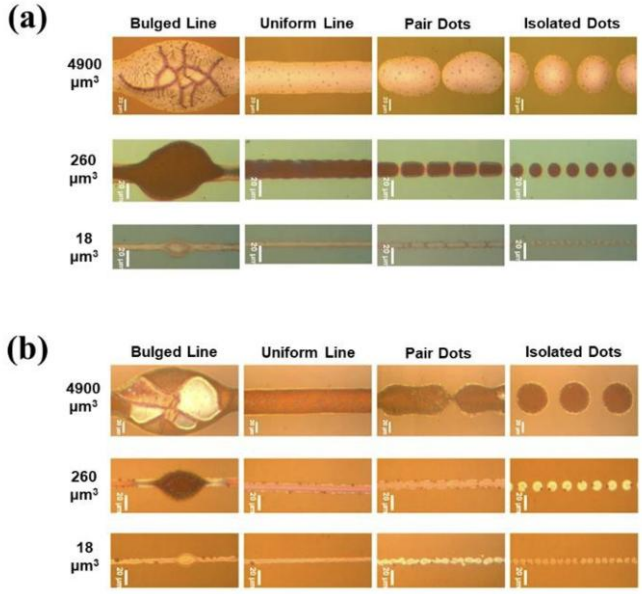

Figure 4. (a) The illustration of dots and lines formations. (b) The description of the formation parameters

Several normalized variables are defined to simplify the expression. α is the normalized variable comparing the cube of the droplet diameter (d_{eqm}^3) and the droplet volume (V_D), as written in equation (3a). The value of α depends on the advanced contact angle of a droplet (θa) [23, 24], as expressed in the equation (3b).

$$\alpha = \frac{{d_{eqm}}^3}{V_D} \tag{3a}$$

$$\alpha = \frac{48}{\pi\left(tan\frac{\theta_a}{2}\right)\left(3+tan^2\frac{\theta_a}{2}\right)} \tag{3b}$$

A simple geometric model can be constructed to describe relationship between the droplet volume (V_D), the pitch (p), the line width (w), and the contact angle (θ) based on volume conservation. The expression for the line width (w) as a function of the pitch (p), the droplet volume (V_D), and the contact angle (θ) is shown in the equation (4).

$$w = \frac{4V_D}{p\left(\frac{\theta}{sin^2\theta} - \frac{cos\theta}{sin\theta}\right)} \tag{4}$$

The advanced contact angle (θ_a) and the contact angle (θ) could be calculated based on the equation (3) and the equation (4), respectively, as shown in the Table 1. The droplet volumes were measured from the 3D profiler images, while the values of the droplet diameters and the line widths were measured from the optical microscopic images. When droplets coalesced together to form a line, the contact angle increased, as indicated by the value of the advanced contact angle, which was always smaller than the value of the contact angle. The results also showed that higher droplet volumes caused both the advanced contact angle and the contact angle to decrease. This phenomenon can be explained by the influence of line tension (the force per unit length along the contact line) at micro or nanoscale. When droplet volume is getting smaller, the line tension becomes more dominant that causes increase in the contact angle [25, 26].

Table 1. Values of derived parameters of all printed dots and lines

Substrate	V_D (μm³)	d_{eqm} (μm)	α	θ_a (degree)	θ (degree)
SiO_2	18	10.04	56.2	10.3	10.6
SiO_2	260	29.30	96.7	6.0	6.6
SiO_2	4900	85.97	129.7	4.5	4.5
Glass	18	9.78	52.0	11.1	11.5
Glass	260	30.18	105.7	5.5	7.1
Glass	4900	97.34	188.2	3.1	4.1

By combining equations (2), (3a), and (4), a relationship between the normalized pitch (p∗) and the line width (w) of the printed line using different droplet volumes could be derived, as shown in equation (5). Figure 5(a) and Figure 5(b) show the line width as a function of the normalized pitch and the droplet volume for lines printed on the SiO_2 substrate and the glass

substrate, respectively. The drop spacing (the pitch) can be controlled by varying the pulse frequency or the printing velocity. The figures show that decreasing the drop spacing and increasing the droplet volume could increase the line width.

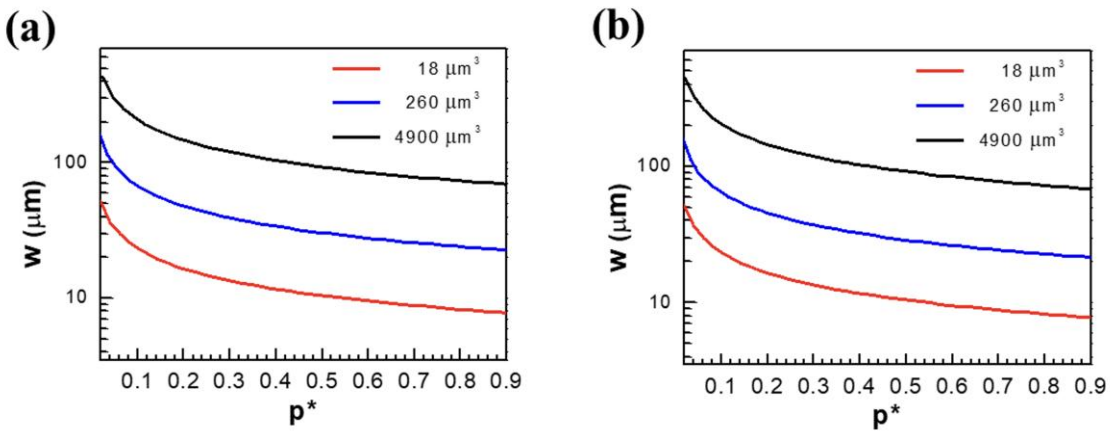

Figure 5. The relationship between the normalized pitch (p*) and the line width (w) of lines formed by droplets with different volumes on: (a) the SiO_2 substrate and (b) the glass substrate.

As shown in the Figure 6, the coalescence of a newly deposited droplet with the line will generate axial flow, which is the flow along the line driven by the pressure difference. In the bulged line, the lowest pressure points are in the bulges. As modelled by Stringer and Derby [11], the rate of axial flow (Q) is proportional to the shape factor (S), the pressure difference (ΔP), and the square of the cross-sectional area (A); it is inversely proportional to the dynamic viscosity of the liquid ink (η) and the droplet spacing (p), as expressed in the equation (6a). The expressions for the cross-sectional area, the pressure difference, and the shape factor are shown in the equations (6b), (6c), and (6d), respectively. θ is the contact angle of the line with the substrate. When a bulge forms, the dynamic contact angle becomes less than the contact angle. This condition can eliminate the driving force required for capillary spreading within the line.

$$Q = \frac{4S\Delta PA^2}{\eta p} \tag{6a}$$

$$A = \frac{V_D}{p} \tag{6b}$$

$$\Delta P = P_f - P_b = \frac{2\sigma sin\theta_a}{d_{eqm}} \frac{w^* - 1}{w^*} \tag{6c}$$

$$S = \frac{\theta - sin\theta cos\theta}{8(sin\theta + \theta)^2} \tag{6d}$$

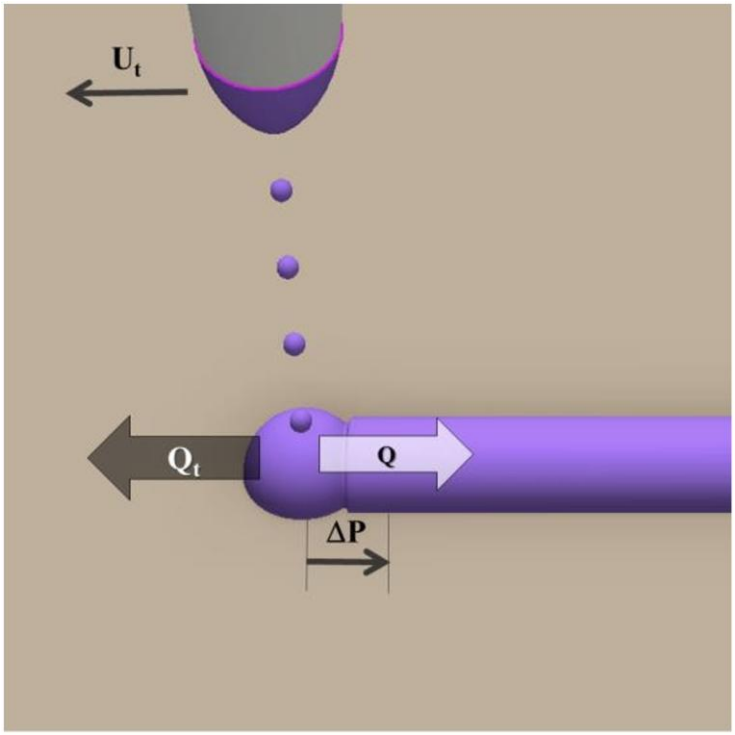

Figure 6. Schematic of fluid flows: *the axial flow* (Q) and *the traverse flow* (Q_t)

On the other hand, during the printing process, the movement of the nozzle with a specified traverse velocity (U_t) generates traverse flow in the opposite direction to the axial flow. The rate of the traverse flow (Q_t) is defined in the equation (7). When the axial flow rate is greater than the traverse flow rate, a new droplet prefers to flow along the bead to a low-pressure area rather than spreading the bead. In this condition, a bulged line will be formed [24]. Conversely, when the traverse flow rate equals or exceeds the axial flow rate, the axial flow can be balanced by the traverse flow, preventing the formation of bulges. This condition is defined as the stable condition, as expressed in equation (8).

$$Q_t = V_D f = \frac{V_D U_t}{p} \tag{7}$$

$$Q_t \geq Q \tag{8}$$

By combining equations (6a), (6b), (6c), (7), and (8), the minimum printing speed in normalized form (U_{t,min^*}) to achieve a stable condition can be described, as shown in equations (9a), (9b), and (9c), where U_t, U_t^*, η, σ, and V_D represent the printing speed, the normalized printing speed, the viscosity of the liquid ink, the surface tension of the liquid ink, and the droplet volume, respectively. Figure 7(a) and Figure 7(b) show the minimum normalized printing speed as a function of the normalized pitch on the SiO_2 substrate and the glass substrate.

Higher droplet volumes required lower normalized minimum printing speeds due to their lower contact angles.

$$U_t{}^* \geq U_{t,min}{}^* \tag{9a}$$

$$U_t{}^* = \frac{\eta U_t}{\sigma} \tag{9b}$$

$$\Delta P = P_f - P_b = \frac{8S\,sin\theta}{a(p^*)^2}\left(\frac{w^*-1}{w^*}\right) \tag{9c}$$

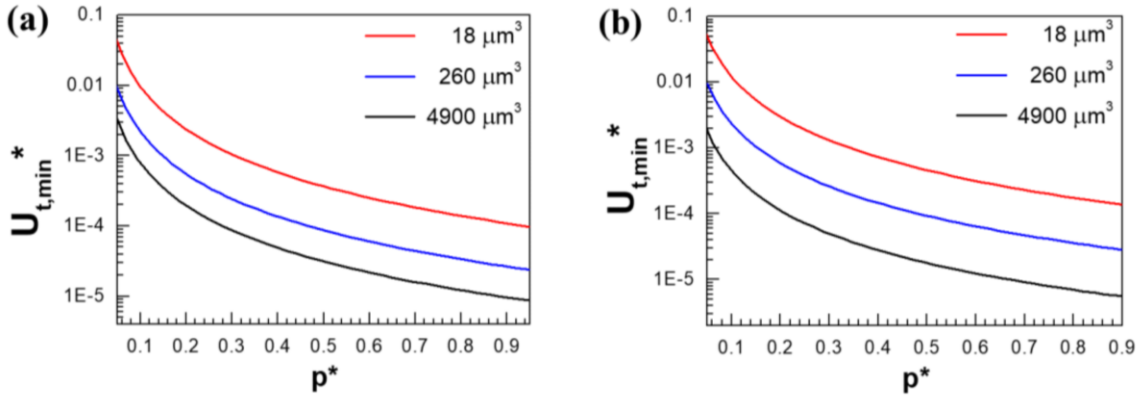

Figure 7. The minimum normalized printing speed as a function of the normalized pitch on: a) the SiO_2 substrate and b) the glass substrate

The remaining fluid flowed from the higher-pressure area into the lower pressure area, resulting in excessive amounts of liquid being generated. A schematic of a bulged line is shown in Figure 8(a). A bulged line has two main parts: the ridge and the bulge. The bulges were formed periodically, and the distance between bulges was determined by the printing velocity and the droplet spacing [27]. By combining the equations (6a), (6b), (6c), (7), and (8), the minimum printing speed in normalized form (U_{t,min^*}) to achieve a stable condition can be described, as shown in equations (9a), (9b), and (9c), where U_{t^*}, U_{t,min^*}, η, σ, and V_D represent the printing speed, the normalized printing speed, the viscosity of the liquid ink, the surface tension of the liquid ink, and the droplet volume, respectively. Equation (7), (8) and (9a) are important and correlated, because they determine the minimum speed (or the minimum flow rate) to prevent the bulging.

In this research, the bulging ratio (BR) is defined as the ratio between the ridge width (w_{ridge}) and the bulge width (w_{bulge}), as expressed in equation (10). The bulging ratio number allows for the observation of bulge growth. Figure 8(b) and Figure 8(c) show the bulging ratio as a function of the normalized pitch and the droplet volume on the SiO_2 substrate and the glass substrate, respectively.

$$BR = \frac{w_{ridge}}{w_{bulge}} \quad (10)$$

Figures 7(a) and 7(b) show the minimum normalized printing speed as a function of the normalized pitch on the SiO_2 substrate and the glass substrate. Higher droplet volumes required lower normalized minimum printing speeds due to their lower contact angles.

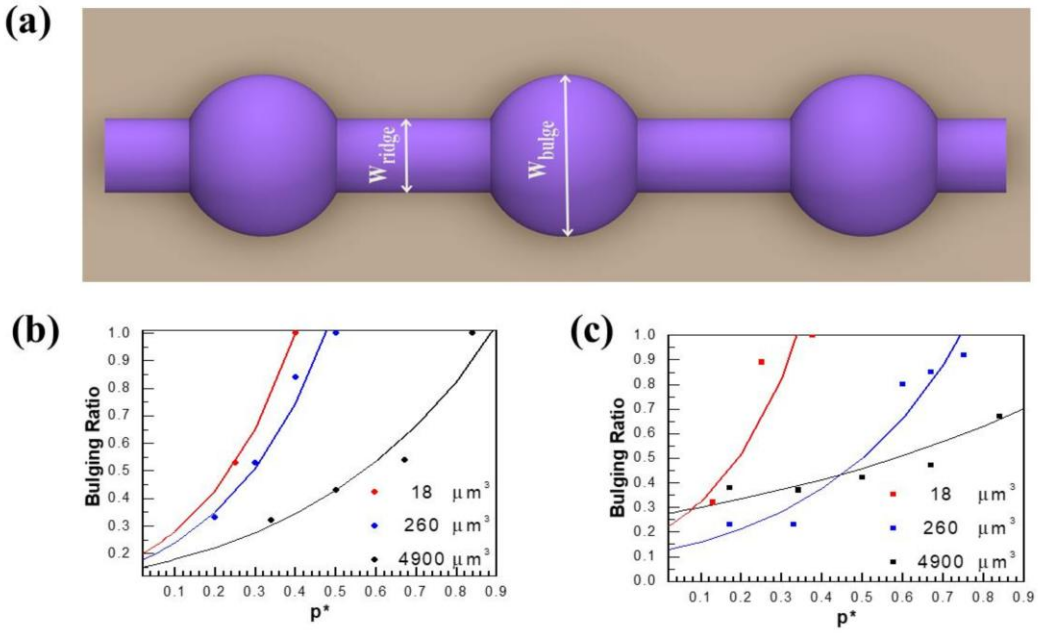

Figure 8. (a) Schematic of the bulging ratio. (b) The bulging ratio as a function of the normalized pitch printed on the SiO_2 substrate using droplets with different volumes. (c) The bulging ratio as a function of the normalized pitch printed on the glass substrate using droplets with different volumes.

Several geometrical patterns could be made by connecting printed lines, as shown in Figure 9(a) and Figure 9(b). Figure 9(a) shows several geometrical patterns printed by DoD of silver nanoparticle ink. Figure 9(b) illustrates electrical split ring resonator patterns achieved by controlling the line width. The electrical split ring resonator structures at the micrometre scale were important for creating electromagnetic resonance and were useful for various applications, such as generating a negative index property [28] or detecting microorganisms [29]. By increasing the line width, bulges were formed on the pattern edges. The bulges on the pattern edges could be minimized or removed by using a smaller line width to reduce the excessive flow to the edges of the patterns.

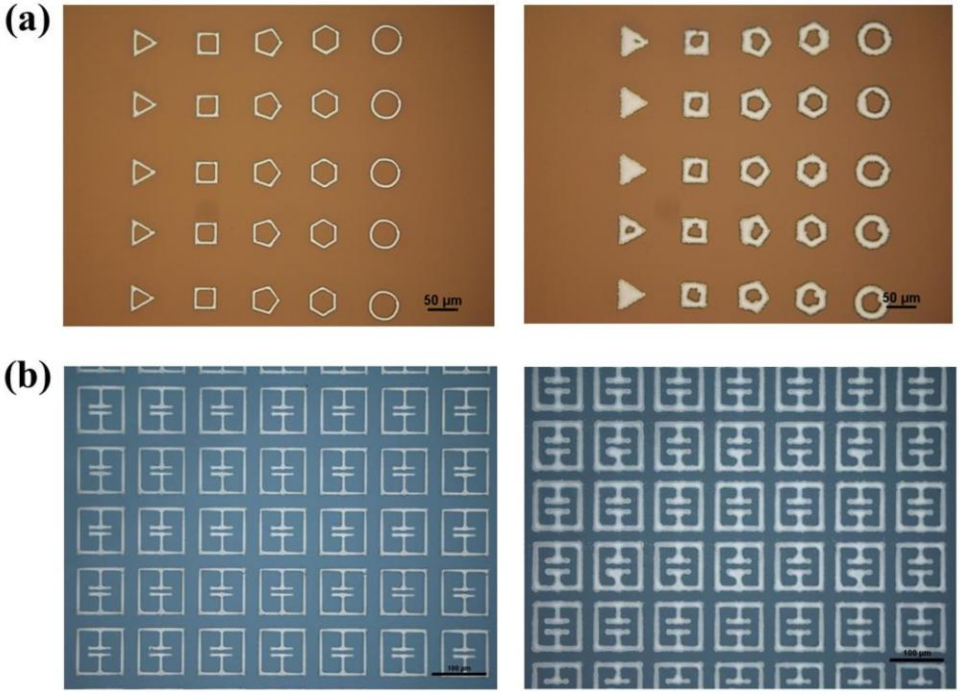

Figure 9. (a) Various geometrical patterns with different line widths, (b) Electrical Split Ring Resonator (ESRR) structures with different line widths.

Conclusion

We have investigated the formation of dots and lines printed using DoD EHD jet printing. Different droplet volumes could be generated on the dielectric substrates. Experimental results showed that dots and lines could be deposited for all droplet volumes by varying the droplet spacing, which could be controlled by adjusting the printing speed or the period of the pulsed electrical signal. When droplets were deposited, the remaining charges on the substrate could significantly affect dot formation, leading to deviations in dot deposition. Increasing the deposited droplet volumes or decreasing the substrate thickness could improve dot formation to create a uniform dot pattern. However, the remaining charges on the substrate did not significantly affect line formation, as the fluid flow dominated, resulting in uniform coalescence of droplets. Stability analysis of line formation revealed that using larger droplet volumes allowed the minimum printing speed for creating uniform lines to be decreased, as the larger droplet volume resulted in a smaller contact angle. By connecting uniform lines, various patterns such as squares or electrical split ring resonators at the micrometre scale could be formed. The uniformity of patterns could be improved by using a smaller line width to reduce excessive flow to the edges of the geometrical pattern.

Acknowledgment

We acknowledge the Multiphysics Nanofluidics Laboratory (MNFL) Sungkyunkwan University which supports facilities and materials to perform experiments and analysis. We also acknowledge Universitas Gadjah Mada (UGM) through *Capstone Program* and *Hibah Penelitian DTNTF* for the support of this collaborative research.

References

[1] Y. Jang, I. H. Tambunan, H. Tak, V. D. Nguyen, T. Kang, and D. Byun, "Non-contact printing of high aspect ratio Ag electrodes for polycrystalline silicone solar cell with electrohydrodynamic jet printing," *Appl. Phys. Lett.*, vol. 102, p. 123901, Mar. 2013.

[2] H. T. Yudistira, A. P. Tenggara, V. D. Nguyen, T. T. Kim, F. D. Prasetyo, C.-G. Choi, M. Choi, and D. Byun, "Fabrication of terahertz metamaterial with high refractive index using high-resolution electrohydrodynamic jet printing," *Appl. Phys. Lett.*, vol. 103, no. 21, p. 211106, Nov. 2013.

[3] H. T. Yudistira, A. P. Tenggara, S. S. Oh, V. D. Nguyen, M. Choi, C.-G. Choi, and D. Byun, "High-resolution electrohydrodynamic jet printing for the direct fabrication of 3D multilayer terahertz metamaterial of high refractive index," *J. Micromech. Microeng.*, vol. 25, no. 4, p. 045006, Apr. 2015.

[4] S. N. Jayasinghe, A. N. Qureshi, and P. A. M. Eagles, "Electrohydrodynamic jet processing: an advanced electric-field-driven jetting phenomenon for processing living cells," *Small*, vol. 2, no. 2, pp. 216–219, Feb. 2006.

[5] C. Cong, X. Li, W. Xiao, J. Li, M. Jin, S. H. Kim, and P. Zhang, "Electrohydrodynamic printing for demanding devices: A review of processing and applications," *Nanotechnol. Rev.*, vol. 11, no. 1, pp. 3305–3334, 2022.

[6] H.-J. Kwon, J. Hong, S. Y. Nam, H. H. Choi, X. Li, Y. J. Jeong, and S. H. Kim, "Overview of recent progress in electrohydrodynamic jet printing in practical printed electronics: focus on the variety of printable materials for each component," *Mater. Adv.*, vol. 2, no. 17, pp. 5593–5615, 2021.

[7] A. Ramon, I. Liashenko, J. Rosell-Llompart, and A. Cabot, "On the Stability of Electrohydrodynamic Jet Printing Using Poly(ethylene oxide) Solvent-Based Inks," *Nanomaterials*, vol. 14, no. 3, p. 273, 2024.

[8] H. T. Yudistira, V. D. Nguyen, P. Dutta, and D. Byun, "Flight behavior of charged droplets in electrohydrodynamic inkjet printing," *Appl. Phys. Lett.*, vol. 96, no. 2, p. 023503, Jan. 2010.

[9] H. T. Yudistira, V. D. Nguyen, S. B. Q. Tran, T. S. Kang, J. K. Park, and D. Byun, "Retreat behavior of a charged droplet for electrohydrodynamic inkjet printing," *Appl. Phys. Lett.*, vol. 98, no. 8, p. 083501, Feb. 2011.

[10] J. Park and J. Hwang, "Fabrication of a flexible Ag-grid transparent electrode using AC based electrohydrodynamic jet printing," *J. Phys. D: Appl. Phys.*, vol. 47, no. 40, p. 405102, Oct. 2014.

[11] H.-J. Kwon, J. Hong, S. Y. Nam, H. H. Choi, X. Li, Y. J. Jeong, and S. H. Kim, "Overview of recent progress in electrohydrodynamic jet printing in practical printed electronics: focus

on the variety of printable materials for each component," *Mater. Adv.*, vol. 2, no. 17, pp. 5593–5615, 2021.

[12] H. T. Yudistira, V. D. Nguyen, P. Dutta, and D. Byun, "Flight behavior of charged droplets in electrohydrodynamic inkjet printing," *Appl. Phys. Lett.*, vol. 96, no. 2, p. 023503, Jan. 2010.

[13] H. T. Yudistira, V. D. Nguyen, S. B. Q. Tran, T. S. Kang, J. K. Park, and D. Byun, "Retreat behavior of a charged droplet for electrohydrodynamic inkjet printing," *Appl. Phys. Lett.*, vol. 98, no. 8, p. 083501, Feb. 2011.

[14] N. Mkhize and H. Bhaskaran, "Electrohydrodynamic jet printing: Introductory concepts and considerations," *Small Sci.*, vol. 2, no. 2, p. 2100073, Feb. 2022.

[15] J. Yang, P. He, and B. Derby, "Stability bounds for micron scale Ag conductor lines produced by electrohydrodynamic inkjet printing," *ACS Appl. Mater. Interfaces*, vol. 14, no. 34, pp. 39601–39609, Aug. 2022.

[16] P. Ren, Y. Liu, R. Song, B. O'Connor, J. Dong, and Y. Zhu, "Achieving high-resolution electrohydrodynamic printing of nanowires on elastomeric substrates through surface modification," *ACS Appl. Electron. Mater.*, vol. 3, no. 1, pp. 192–202, Jan. 2021.

[17] N. Sahoo, D. Samanta, and P. Dhar, "Electrohydrodynamics of dielectric droplet collision on different wettability surfaces," *Phys. Fluids*, vol. 33, no. 11, p. 112108, Nov. 2021.

[18] S. Cai, Y. Sun, Z. Wang, W. Yang, X. Li, and H. Yu, "Mechanisms, influencing factors, and applications of electrohydrodynamic jet printing," *Nanotechnol. Rev.*, vol. 10, no. 1, pp. 1046–1078, Sep. 2021.

[19] Y. Jiang, D. Ye, A. Li, B. Zhang, W. Han, X. Niu, M. Zeng, L. Guo, G. Zhang, Z. Yin, and Y. Huang, "Transient charge-driven 3D conformal printing via pulsed-plasma impingement," Proc. Natl. Acad. Sci. U.S.A., vol. 121, no. 22, p. e2402135121, May 2024.

[20] K. H. Choi, M. Zubair, and H. W. Dang, "Characterization of flexible temperature sensor fabricated through drop-on-demand electrohydrodynamics patterning," *Jpn. J. Appl. Phys.*, vol. 53, no. 5S3, p. 05HB02, May 2014.

[21] B. Zhang, B. Seong, J. Lee, V. D. Nguyen, D. Cho, and D. Byun, "One-step nanoscale electrohydrodynamic inkjet three-dimensional printing technique with spontaneous Joule heating," *ACS Appl. Mater. Interfaces*, vol. 9, no. 35, pp. 29380–29387, Sep. 2017.

[22] M. S. Onses, E. Sutanto, P. M. Ferreira, A. G. Alleyne, and J. A. Rogers, "Mechanisms, capabilities, and applications of high-resolution electrohydrodynamic jet printing," *Small*, vol. 11, no. 34, pp. 4237–4266, Sep. 2015.

[23] D. Soltman and V. Subramanian, "Inkjet-printed line morphologies and temperature control of the coffee ring effect," *Langmuir*, vol. 24, no. 5, pp. 2224–2231, Mar. 2008.

[24] J. Stringer and B. Derby, "Formation and stability of lines produced by inkjet printing," *Langmuir*, vol. 26, no. 12, pp. 10365–10372, Jun. 2010.

[25] W. Klauser, F. T. von Kleist-Retzow, and S. Fatikow, "Line tension and drop size dependence of contact angle at the nanoscale," *Nanomaterials*, vol. 12, no. 3, p. 369, Jan. 2022.

[26] M. Iwamatsu and H. Mori, "Effect of line tension on axisymmetric nanoscale capillary bridges at the liquid-vapor equilibrium," *Phys. Rev. E*, vol. 100, no. 4, p. 042802, Oct. 2019.

[27] P. C. Duineveld, "The stability of ink-jet printed lines of liquid with zero receding contact angle on a homogeneous substrate," *J. Fluid Mech.*, vol. 477, pp. 175–200, Mar. 2003.

[28] W. J. Padilla, M. T. Aronsson, C. Highstrete, M. Lee, A. J. Taylor, and R. D. Averitt, "Electrically resonant terahertz metamaterials: Theoretical and experimental investigations," *Phys. Rev. B*, vol. 75, no. 4, p. 041102, Jan. 2007.

[29] S. J. Park, J. T. Hong, S. J. Choi, H. S. Kim, W. K. Park, S. T. Han, J. Y. Park, S. Lee, D. S. Kim, and Y. H. Ahn, "Detection of microorganisms using terahertz metamaterials," *Sci. Rep.*, vol. 4, p. 4988, May 2014.